Research Article | Vol. 33, No. 14 / 14 Jul 2025 / Optics Express 30328
Optics EXPRESS

Surface lattice resonances for high-performance sensing: a study on gold nanoparticle arrays

URSULA F. S. ROGGERO,[1,†] CARLOS J. ROJAS-BEJARANO,[2,†] CÉSAR A. HERREÑO-FIERRO,[3] ANDREAS SEIFERT,[4,5] AITZOL GARCIA-ETXARRI,[5,6] HUGO E. HERN NDEZ-FIGUEROA,[1] AND MARIO ZAPATA-HERRERA[6,*]

[1] *University of Campinas, School of Electrical and Computer Engineering, Av Albert Einstein 400, 13083-852 Campinas, São Paulo, Brazil*
[2] *Universidad Central, Carrera 5 n ° 21-38, Facultad de Ingeniería y Ciencias Básicas, Bogotá, Colombia*
[3] *Universidad Distrital Francisco José de Caldas, Carrera 3 # 26A-40 PCLF 110311, Bogotá, Colombia*
[4] *CIC nanoGUNE BRTA, 20018 San Sebastián, Spain*
[5] *IKERBASQUE, Basque Foundation for Science, 48013 Bilbao, Spain*
[6] *Donostia International Physics Center, Paseo Manuel de Lardizábal 5 20018, Donostia-San Sebastián, Spain*
[†] These authors contributed equally
[*] *mario zapatah@ehu eus*

Abstract: In this study, localized surface plasmon resonances and diffractive coupling effects in periodic arrays of gold nanoparticles, which give rise to surface lattice resonances, were systematically explored Using the finite element method simulations in COMSOL Multiphysics, we analyzed how nanoparticle geometry and lattice configuration affected the quality factor and sensitivity Compared to isolated nanoparticles, periodic arrays of nanospheres, nanodisks, and nanorods exhibited significantly enhanced sensing capabilities due to diffractive coupling, achieving quality factors an order of magnitude higher and bulk sensitivity improvements exceeding 100 nm/RIU This article confirms experimentally the emergence of hybrid spectral features in such periodic arrays, resulting in narrower resonances and enhanced sensing performance A proof-of-concept sensor based on a 600-nm periodic gold nanodisk array demonstrates reliable sensitivity, validating that even simple geometries can achieve high performance by harnessing the collective effects of periodicity These findings emphasize the strong potential of gold nanoparticle arrays in high-performance sensing applications empowered by surface lattice resonances

1. Introduction

Plasmonics exploits the exceptional ability of metallic nanostructures to confine and manipulate light at scales below the diffraction limit, enabling a broad spectrum of applications, including enhanced photoluminescence [1], optical nanoantennas [2], plasmon-enhanced photodetection [3–5], photochemistry [6], nonlinear optics [7], and energy harvesting [8] It focuses on the collective resonant oscillations of conduction electrons in metals, referred to as surface plasmon resonances, which are triggered by the light-matter interactions at the nanoscale In particular, when light interacts with a metallic nanoparticle (NP), the conduction electrons oscillate coherently under the influence of the incident electromagnetic field, leading to localized surface plasmon resonances (LSPR) [9], typically characterized by means of its scattering, absorption and extinction spectra The resonance wavelength of this LSPR is mainly determined by the geometry and material properties of the nanoparticle as well as the optical properties of the surrounding environment [1]

564444 https://doi.org/10.1364/OE.564444
Journal © 2025 Received 7 May 2025; revised 30 May 2025; accepted 13 Jun 2025; published 10 Jul 2025

Optics EXPRESS

Plasmonic resonances in isolated nanoparticles produce unique optical phenomena, including highly localized and enhanced electric fields, typically in the visible (VIS) to near-infrared (NIR) spectrum for nanoparticles made of noble metals (gold or silver) These effects hold an enormous potential for technological applications These applications include generating magneto-optical responses in the VIS and NIR spectral range [10–13], highly sensitive molecular detection [14–17], high-resolution imaging [18], nanoscale electronics [19], high-speed telecommunications [20], efficient solar energy conversion [21,22], catalytic processes [23], among others

The strong confinement of the electric field using plasmonic nanostructures makes them excellent candidates as transducers in sensing applications [5,24–26] Combined with spectral shifts induced by changes in the surrounding dielectric medium, these effects form the basis of the sensing mechanism in plasmonic biosensors [27]

A critical parameter for assessing the performance of plasmonic systems is the quality factor (or Q factor), defined as the ratio of energy stored to energy lost per oscillation cycle For LSPRs, the Q factor is expressed as $Q \quad \lambda_{res}/ \quad \lambda$, where λ_{res} is the resonance wavelength, and λ is the full width at half maximum (FWHM) of the resonance peak LSPRs in isolated NPs typically exhibit Q factors ~10, limiting their utility in many applications While the Q factor is predominantly governed by the intrinsic properties of the metal, it can be significantly enhanced through structural and compositional design [28]

Periodic arrangements of metallic NPs offer a promising solution to overcome the limitations of isolated LSPRs In such systems, electromagnetic fields associated with the LSPR modes of individual NPs mediate interactions between neighboring NPs Two types of coupling mechanisms are prevalent: on one hand, near-field coupling occurs in densely packed NPs through hybridization of plasmonic modes, resulting in spectral shifts and the formation of new, hybridized, modes Antisymmetric hybridized modes, while showing narrower resonances, are often non-radiating and challenging to excite [29–33] On the other hand, far-field coupling arises in 2D periodic lattices where the lattice constant is comparable to the incident light's wavelength Under these conditions, scattered fields from individual NPs interfere constructively with the incident wave, leading to the formation of surface lattice resonances (SLRs) These resonances exhibit substantially higher Q factors than isolated NPs due to diffractive coupling and enhanced sharpness of the resonance peak [34] In addition, while recent advances in bound states in the continuum (BICs) have demonstrated Q-factors exceeding 1000 in engineered metasurfaces through symmetry protection mechanisms [35,36], our study focuses on classical SLRs in gold nanodisk arrays Here, the goal is not to achieve ultra-high Q-factors but to elucidate the impact of periodicity in simple, experimentally feasible geometries Extensive research has demonstrated that careful tuning of NP size, shape, and lattice constant optimizes the optical response of periodic arrays, making them ideal for applications requiring high sensitivity [37–41] Notably, SLRs are highly sensitive to variations in the surrounding dielectric environment, highlighting their potential for plasmonic sensing [42]

In this work, we investigate a variety of structural parameters governing the spectral position, Q factor, and sensitivity of SLRs in periodic arrays of gold NPs Using finite element method (FEM) simulations implemented in COMSOL Multiphysics [43], we examine the influence of the NP geometry and the lattice constant on the optical response of these arrays comparing them to their isolated NP counterparts While the principles underlying surface lattice resonances (SLRs) and their application in sensing are well established, this work presents a systematic study of how the interplay between nanoparticle geometry and lattice configuration affects the sensing performance of plasmonic arrays We analyze and compare the behavior of nanospheres, nanodisks, and nanorods arranged in periodic arrays, focusing on quality factor, bulk sensitivity, and figure of merit (FoM) Our results reveal that periodic NP arrays with optimized geometries can achieve Q factors one order of magnitude higher than those of isolated NPs, with bulk sensitivity improvements higher than 100 nm/RIU compared to LSPRs Additionally, we validate

Optics EXPRESS

our theoretical findings experimentally by fabricating a proof-of-concept sensor based on a periodic array of gold nanodisks by using electron beam lithography (EBL) This study presents a case analysis of a simple nanodisk array to evaluate the impact of periodicity and SLR formation on sensing performance, rather than an exhaustive optimization across the multidimensional parameter space Our work validates different approaches obtained widely in the community using a variety of nanoplasmonic scenarios where complex structures are involved [17,36,44–50] In our case, using gold nanodisks arrays, the performance in terms of sensibility is very large compared with its isolated counterpart

The article is structured as follows: first, we describe the theoretical approach, which consists of the computational model, the numerical method to investigate the optical response of periodic arrays, and the corresponding theoretical results Then we present the experimental approach, which consists of the experimental methods and results, focusing on the interplay between lattice structure, plasmon modes, and SLR sensitivity Finally, we summarize the results and discuss future prospects for plasmonic sensing applications

2. Theoretical approach

2.1. Computational model

Using the Finite Element Method (FEM), implemented in the COMSOL Multiphysics suite [42], we solve the Maxwell's equations and obtain the optical response Figure 1 presents the two systems modeled in our analysis: isolated plasmonic nanoparticles (NPs) and 2D nanoparticle arrays Figures 1(a) and 1(c) schematically illustrate an isolated gold nanoparticle and its corresponding computational simulation box, respectively The figure depicts a nanodisk as a NP example Nevertheless, our study analyzes the optical response of nanodisks, nanospheres and nanorods Figures 1(b) and 1(d) depict a periodic square array of NPs with a lattice constant Λ, showing both, the schematic representation of the system and its corresponding computational implementation In both cases, the isolated NP and the NP array are embedded in an optical medium with refractive index n The lattice constant and geometric parameters for the three nanoparticle shapes studied (nanospheres, nanodisks, and nanorods) were selected to ensure that the resulting resonances fall within the visible and near-infrared range, and to match practical fabrication constraints While a full parametric study of these variables could provide additional insight into optimization strategies, our aim here is to perform a comparative analysis across common, experimentally accessible geometries using representative conditions A broader investigation of how lattice constants and aspect ratios affect sensor performance remains an interesting direction for future studies

For the isolated system, a gold NP was placed in a spherical computational domain enclosed by a PML under the incidence of a plane wave We calculate the extinction cross-section σ_{ext} as the sum of the scattering cross-section σ_{scat} and the absorption cross-section σ_{abs}, which are correspondingly calculated as

$$\sigma_{scat} \quad \frac{1}{|S_{in}|} \int_s S_{scat} \cdot ds, \tag{1}$$

and

$$\sigma_{abs} \quad \frac{1}{|S_{in}|} \int_s S \cdot ds \tag{2}$$

In Eqs (1) and (2), S corresponds to the Poynting vector, and the subscripts "in" and "scat" refer to the incident and scattered components of S The factor ds represents the differential of the integration surface Each cross-section (expressed in units of area) quantifies the likelihood of extinction, absorption, or scattering at a specific wavelength These quantities are directly related to the nanoparticle's polarizability, which governs its plasmonic resonance behavior [9] For the gold NP array, Floquet periodic boundary conditions are applied to simulate the periodic

Optics EXPRESS

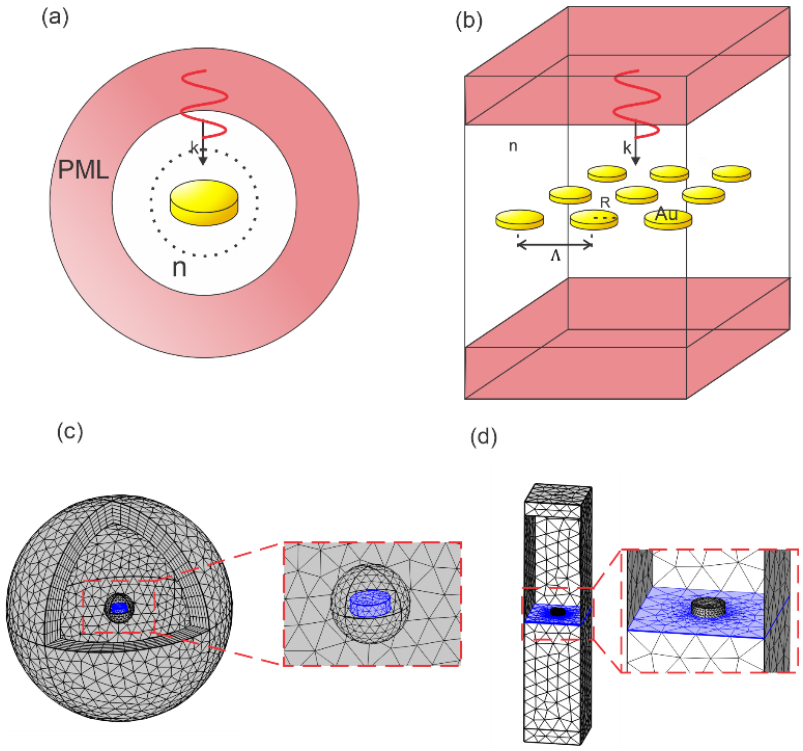

Fig. 1. Schematic and computational models for studying the optical response of isolated and periodic gold nanoparticle arrays (a) Isolated gold nanodisk placed at the center of the simulation domain, surrounded by an optical medium with refractive index n (white region) A perfectly matched layer (PML, red region) encloses the computational box to prevent spurious reflections (b) Square array of gold nanodisks with lattice constant Λ, where PMLs (red regions) are placed at the top and bottom boundaries, and Floquet periodic boundary conditions are applied to the four side walls to simulate an infinite two-dimensional array Computational COMSOL Multiphysics model of the (c) isolated nanodisk, and (d) periodic nanodisk array

nature of the system, modeling an ideal infinite array This approach is widely adopted in the literature and provides a good approximation when the optical spot size is much larger than the array unit cell, as in our experimental case While real-world devices are finite and can exhibit edge effects or structural imperfections, their impact is minimal under such conditions

A full analysis of finite-size corrections or disorder effects lies beyond the scope of this study, which focuses on idealized conditions to elucidate fundamental trends in SLR-based sensor performance In addition, the array is excited by linearly polarized light, and PML boundaries are placed at the top and bottom of the computational domain to absorb outgoing waves and avoid spurious reflections Within this model, three key optical quantities are calculated: reflectance (R), transmittance (T), and absorbance (A)

2.2. *Theoretical results: surface lattice resonances and their enhanced sensing capa bilities*

To evaluate the influence of the surrounding refractive index on SLRs, we define the bulk sensitivity S as the spectral shift of the resonance wavelength (λ_{res}) per unit change in the

Optics EXPRESS

surrounding medium's refractive index (n) as

$$S \quad \lambda_{res}/\ n \tag{3}$$

It is important to note that bulk sensitivity quantifies the sensor's response to a uniform change in the refractive index of the surrounding medium, such as when the sensor is immersed in different liquids This parameter is especially useful for evaluating optical sensors that are not biofunctionalized, meaning the surface of the nanoparticles has not been chemically treated to capture specific molecules This distinguishes bulk sensitivity, which reflects overall environmental changes, from surface sensitivity, which is characteristic of biosensors designed to detect localized molecular binding near the sensor surface Additionally, we introduce the figure of merit (FoM), which accounts for both sensitivity and spectral linewidth, given by:

$$\text{FoM} \quad S/\ \lambda, \tag{4}$$

where λ corresponds to the full width at half maximum (FWHM) of the resonance The FWHM is a key parameter in SLR-based sensors, as it directly influences the precision with which spectral shifts can be measured Narrower linewidths enhance the sensor's ability to resolve small refractive index changes Therefore, the FoM quantifies the trade-off between sensitivity and spectral linewidth—higher FoM values indicate superior performance in terms of detection accuracy and reliability This is particularly relevant at the proof-of-concept stage, where optimizing both sensitivity and resolution is crucial for practical applications

Figure 2(a) shows the extinction cross-section spectra of three geometries evaluated under both isolated and array conditions The study considers nanospheres (R 50 nm, Λ 420 nm), nanodisks (R 50 nm, H 30 nm, Λ 490 nm), and nanorods (R 30 nm, L 90 nm, Λ 430 nm) The lattice parameters were chosen assuming the condition $|(\lambda_{RA} \quad \lambda_{LSPR})|$ 0 (see Supplement 1 S1, for details)

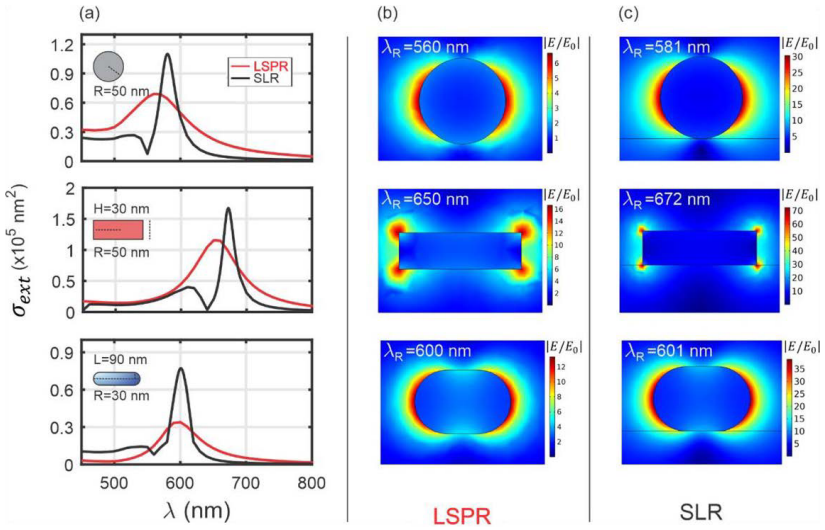

Fig. 2. Influence of lattice effects on the optical response of different gold NP geometries (a) Extinction cross-section spectra of nanospheres (NS), nanodisks (ND), and nanorods (NR) The red and black curves represent isolated and array configurations, respectively Near-field enhancement at resonance wavelengths for each NP under (b) Localized Surface Plasmon Resonance (LSPR) and (c) Surface Lattice Resonance (SLR) conditions

Figures 2(b) and 2(c) illustrate the near-field enhancement $|E/E_0|$ at resonance wavelength of each geometry in isolated and array configuration, respectively The intensity of the incident field

Optics EXPRESS

(E_0) was set to 1 V/m The hotspots around the gold NPs demonstrate the plasmon excitations in both configurations However, the arrays show stronger field confinement, at least four times higher than those of the isolated NPs, suggesting a higher sensitivity Figures 3(a) and 3(b) illustrate, respectively, the numerical results of the spectral shift of the LSPRs calculated for isolated NPs and the SLRs for nanoparticle arrays as a function of the refractive index of the surrounding medium Each point represents the resonance wavelength of each system for its corresponding surrounding refractive index By performing a linear fit to each dataset, we can determine the sensitivity S of each scenario, as shown in Fig 3(c) The array systems exhibit significantly higher sensitivity than their isolated counterparts, with improvements of at least 100 nm/RIU Figure 3(d) shows the Q factors of each system, demonstrating that the array configuration enhances the sharpness of the resonance peak This effect results in higher FoM values, as illustrated in Fig 3(e), since the FoM is directly proportional to sensitivity and inversely proportional to the width of the resonance peak These results highlight the substantial improvements in sensitivity, quality factor, and figure of merit achieved by organizing gold NPs into periodic arrays Figure 3 illustrates that the array of nanodisks consistently shows better results over the three explored quality metrics

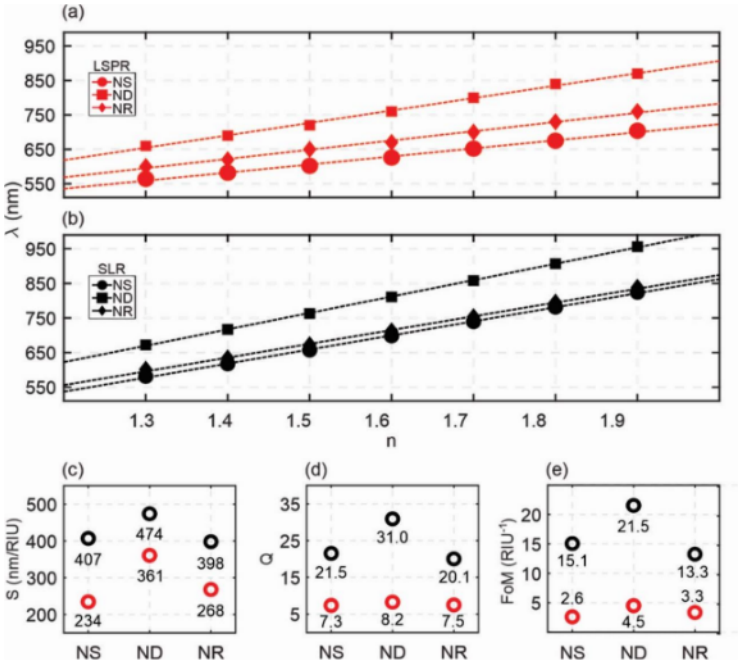

Fig. 3. Sensing performance of isolated and arrayed gold nanoparticles (a) Resonance wavelength as a function of the surrounding refractive index n for isolated nanospheres (NS), nanodisks (ND), and nanorods (NR) (b) The same analysis for NP arrays (c) Sensitivity, (d) Quality factor, and (e) Figure of merit comparison between array (black) and isolated (red) configurations, highlighting the enhancement due to diffractive coupling in periodic arrays

These theoretical simulations show that by carefully tuning the nanoparticle geometry and lattice configuration, it is possible to enhance the Q factor and sensitivity of plasmonic arrays However, these results assume idealized conditions, such as perfect nanoparticle shapes and uniform distributions To validate these predictions, we fabricated gold nanodisk arrays and performed optical characterization experiments to assess their spectral response and sensing capabilities Section 3 presents the experimental methodology and discusses the extent to which our theoretical predictions align with the experimental findings

Optics EXPRESS

It is important to note that we have focused on the case of normal incidence and TM polarization, which is a standard configuration in both experimental and numerical studies involving SLRs However, it is well known that angle of incidence and polarization can significantly influence the optical response of periodic plasmonic structures, potentially leading to tunable or more directional resonances [51] Exploring these effects could further extend the practical applicability of our approach and will be considered in future work

2.3. Effect of substrate asymmetry

In practical sensing applications, plasmonic nanoparticle arrays are typically supported on dielectric substrates and may be embedded within heterogeneous environments These asymmetries influence both the spectral position and the intensity of resonances For example, a higher-index substrate induces a redshift in the plasmon resonance and can redistribute the local electric fields, often directing a significant portion toward the substrate [52–54] While the simulations in this work are performed under symmetric conditions for clarity and generalization, the design strategies and trends reported here remain valid under more realistic conditions A redshift correction can be incorporated when transitioning to experimental setups, without altering the essential conclusions on the relative enhancement of quality factor, sensitivity, and FoM in SLR-based structures

3. Experimental approach

3.1. Methods and fabrication

In this section, we present the experimental results of an array of nanodisks, focusing on the lattice effect on its optical response and demonstrating its good performance as a sensor This geometry was employed due to its superior theoretical metrics in sensitivity, quality factor and figure of merit Moreover, a circular cross-section minimizes the dependence of incident light polarization in the plane transverse to the propagation direction The gold nanodisks were fabricated on indium tin oxide (ITO)-coated glass slides, with a thin layer of titanium to enhance gold adhesion to the substrate, as shown in Fig 4(a) Both periodic square arrays and an aperiodic array were fabricated to analyze the lattice effect The individual elements of both arrays were identical, consisting of nanodisks with a diameter of 225 nm and a height of 45 nm

The schematics in Fig 4(b) and Fig 4(c) illustrate the distribution of the periodic and aperiodic arrays, respectively The periodic arrays were fabricated with lattice constants of 400 nm, 500 nm, and 600 nm, whereas the aperiodic array followed a Fermat's spiral configuration, with the polar coordinates defined by

$$\rho_m \quad \frac{\mathrm{d}}{d_{14}}\sqrt{m}, \tag{5}$$

$$\phi_m \quad m\pi \quad 3 \quad \sqrt{5}\Big), \tag{6}$$

where m is the index of each element in the array, d is the minimum distance between elements - set to 400 nm corresponding to the smallest lattice constant in periodic arrays - and the parameter d_{14} is given by $d_{14} \quad \sqrt{5 \quad 4\cos\phi_3}$

EBL was employed to fabricate the arrays, as it is particularly well-suited for creating large, spatially controlled arrangements The periodic arrays covered a footprint of 2×2 mm^2, containing between 11 and 25 million nanodisks, depending on the lattice period The aperiodic array, with a footprint of 100×100 μm^2, contained 5×10^4 gold nanodisks Figure 4(d) and 4(e) show SEM images of the fabricated periodic and aperiodic arrays, confirming the circular shape of the nanodisks with a mean diameter of 225 nm and their intended distributions

Optics EXPRESS

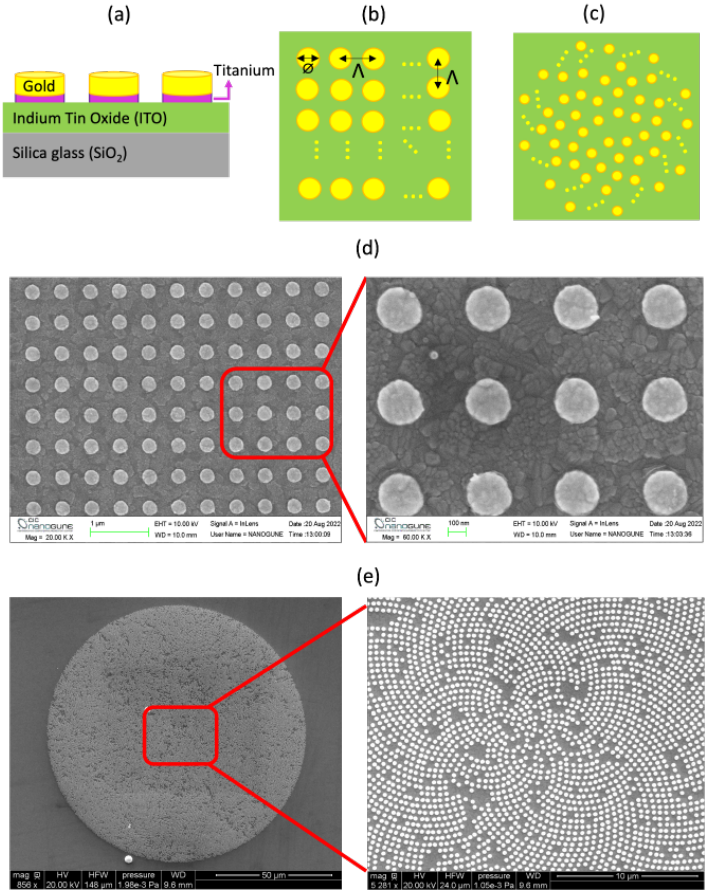

Fig. 4. Schematic of the nanodisk arrays: (a) Side view, (b) Top view of a periodic square array, and (c) Top view of an aperiodic array The nanodisks have a diameter Ø 225 nm and a height h 45 nm SEM images of the fabricated nanodisk arrays: (d) Periodic square array and (e) Aperiodic array

3.2. *Experimental results*

A custom-built spectroscopic setup in transmission configuration was used to optically characterize the nanodisk arrays Figure 5(a) presents the transmittance spectra measured for each fabricated array As expected, a clear difference in the spectral response of the aperiodic array compared to the periodic arrays was observed The aperiodic array (black line) exhibited a broad dip associated with plasmonic resonance, indicative of the LSPR phenomenon, without influence from any lattice effects In contrast, the periodic arrays showed a hybrid spectrum that clearly revealed the lattice effect (SLR), as described previously For Λ 400 nm (orange line), a small non-plasmonic dip around 630 nm was observed It appeared near the broad plasmonic resonance but it did not significantly affect it The array corresponding to Λ 500 nm (yellow line) exhibited two small dips around 550 nm and 705 nm, respectively, with the latter interacting slightly with the plasmonic dip, resulting in a typical Fano-like shape This effect is more pronounced for Λ 600 nm (purple line) in which a small dip at 654 nm is observed, due to the periodic distribution, along with a narrow hybrid resonance dip resulting from the interaction of the LSPR and the diffractively coupled effects, demonstrating the appearance of a clear SLR This result is the most favorable, as narrower plasmonic resonances provide higher figure of merit for

Optics EXPRESS

sensing applications In that sense, Fig 5(b) shows the transmittance of the Λ 600 nm periodic array for two surrounding media with largely different refractive indices: air and water As expected, the first small dip, primarily due to periodic distribution, was slightly affected, showing a small red-shift from 654 nm to 661 nm However, the SLR dip experienced a large red-shift from 907 nm to 957 nm, demonstrating that the plasmonic phenomenon is highly sensitive to variations in the surrounding medium, making the plasmonic arrays excellent candidates for sensing applications

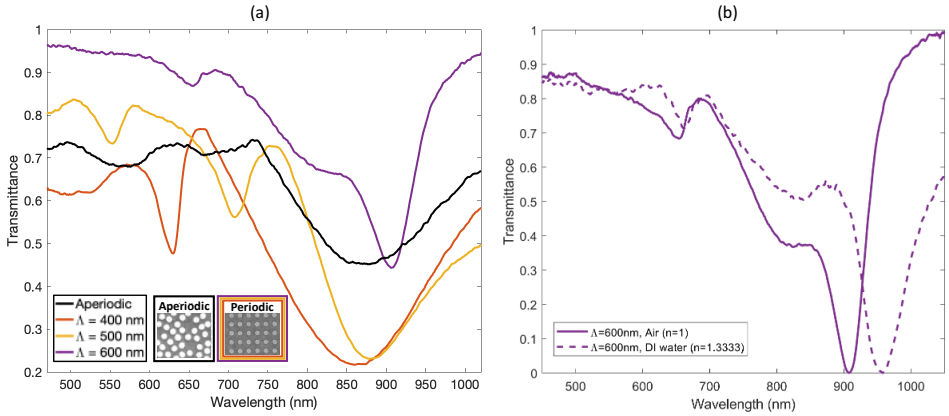

Fig. 5. Optical characterization of periodic and aperiodic nanodisk arrays (a) Measured transmittance spectra of periodic nanodisks arrays (colored curves) with lattice constants of Λ 400 nm, 500 nm, and 600 nm, and an aperiodic array (black curve) (b) Measured transmittance spectra of the 600-nm periodic nanodisk array for two surrounding media: air (n 1) and water (n 1 33)

Furthermore, a proof-of-concept sensing experiment was carried out using this 600-nm periodic gold nanodisk array (Fig 6) During the test, the refractive index of the surrounding medium is changed and the changes in the optical response of the device are determined A micro spectroscopic setup based on an upright microscope (Axio Examiner, Carl Zeiss) was employed for this procedure A halogen lamp (HL-2000, Ocean Optics) with a wavelength range from 360 nm to 2,400 nm and a fiber-coupled CCD spectrometer (Maya2000Pro, Ocean Optics) with a spectral range of 165 nm to 1,100 nm were used Solutions of sucrose (S0389, Sigma-Aldrich) in deionized (DI) water were prepared at concentrations of 2%, 5%, 8%, and 10% to generate varying refractive indices Table 1 shows the refractive index values of the sucrose solutions and their variations relative to pure DI water, which served as the reference

Table 1. Refractive indices of sucrose solutions

Solution	$n_{sucrose}$	$n_{sucrose}$	$n_{sucrose}$	n_{water}
2% sucrose	1 3362	2 90 × 10	3	
5% sucrose	1 3405	7 20 × 10	3	
8% sucrose	1 3449	1 16 × 10	2	
10% sucrose	1 3475	1 42 × 10	2	

In Fig 6(a), we present the transmittance spectra obtained for the reference and the aqueous sucrose solutions As illustrated in the inset, increasing sucrose concentrations caused a red-shift in the resonance dip due to the higher refractive indices of the medium From these measurements, the calibration curve of the device was generated, showing the resonant wavelength shift as a function of the refractive index change (Fig 6(b)) After linear fitting, the experimental sensitivity

Optics EXPRESS

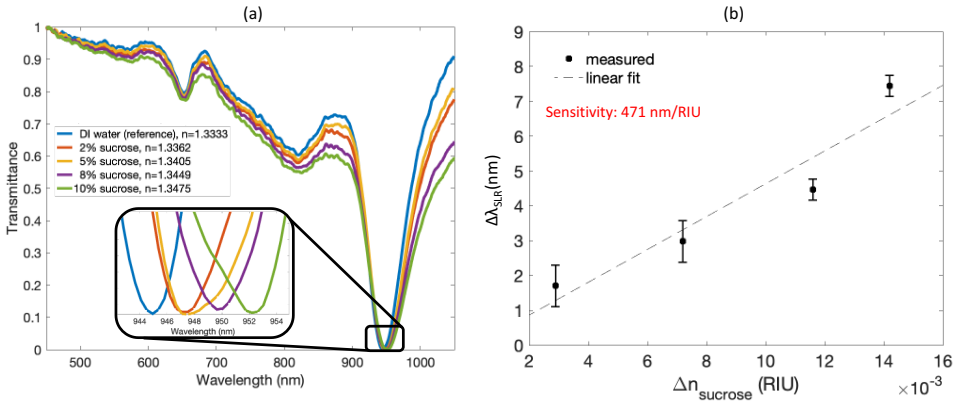

Fig. 6. Experimental results of the 600-nm periodic array of nanodisks as a plasmonic sensor for the refractive index: (a) Transmittance spectra with sucrose solutions at different concentration (curves rescaled from 0 to 1 for better visualization of the wavelength shift) (b) Sensitivity curve (measured points and linear fit)

was determined from the slope of the curve, resulting in a value of 471 nm/RIU, which is in good agreement with the simulated results shown in Fig 3(c) The FWHM was taken from the transmittance curve of the reference (DI water), resulting in 57 nm These values yield the calculated Q factor and figure of merit (FoM) of 16 6 and 8 3 RIU ^{1}, respectively

Despite the excellent agreement between simulated and experimental resonance positions and trends, we observed a significant discrepancy in the quality factor (Q) of the resonances: simulations predict values exceeding 200, while the experimentally measured Q factor for the proof-of-concept device is approximately 16 6 This difference is not unexpected and can be attributed to several well-known factors that arise in the transition from idealized models to fabricated devices 1) Surface roughness and grain boundaries: the fabrication process, particularly electron beam lithography followed by metal deposition and lift-off, introduces nanoscale surface roughness and crystalline grain boundaries in the gold nanodisks These imperfections increase electron scattering and introduce non-radiative losses, effectively broadening the resonance linewidth and reducing the Q factor Such effects are not captured in simulations where the material interfaces are treated as perfectly smooth and crystalline 2) Spatial and geometrical disorder: In practice, there are inevitable deviations from the ideal periodic arrangement assumed in simulations Variations in nanoparticle size, shape, center-to-center distance, or alignment due to fabrication tolerances can cause dephasing and inhomogeneous broadening of the collective resonance These effects diminish the coherence of the surface lattice resonances (SLRs) and lead to a measurable reduction in Q While small, such disorders can critically impact modes that rely on long-range coupling, as in SLRs 3) Finite array size: The simulations assume an infinite array by using Floquet periodic boundary conditions, whereas the experimental structures are finite in size This mismatch has two implications: (i) edge effects can disrupt the coherent build-up of SLRs near the boundaries, and (ii) the finite array length effectively imposes a distribution of momenta, resulting in spectral broadening The illuminated area during measurement is typically smaller than the full array, but large enough that finite-size effects are non-negligible 4) Material model and optical constants: our simulations used literature values for the dielectric function of bulk gold (e g , from Johnson and Christy) However, nanostructured gold, particularly when deposited in thin films, often exhibits increased damping due to surface and interface scattering, reduced grain sizes, and deposition conditions These effects shift and broaden the plasmonic resonance, reducing the Q factor Despite these limitations, the experimental result of Q ≈ 16 6

Optics EXPRESS

represents a substantial improvement compared to isolated nanoparticle resonances and supports the potential of SLR-based platforms for high-performance sensing

The obtained results demonstrate good sensing performance suitable for refractive index detection in liquid environments Table 2 presents a literature benchmark, comparing our sensitivity, FoM, and Q-factor values with representative results from both simple and more complex sensor designs While not all three parameters are reported in every study, the available performance metrics and stated objectives allow for a meaningful comparison with our work

Table 2. Comparative benchmark of the sensitivity, FoM, and Q-factor values with representative results from sensor designs reported in the literature

Configuration	Sensitivity (nm/RIU)	FoM (RIU ^{1})	Q-factor	Goal	Reference
Gold nanodisks	471	8 3	16 6	Good sensing by SLR	This work
Si nanodisks	150	3 8	Not informed	Effective sensing via simple all-dielectric oligomers	K E Chong et al (2017) Ref [50]
Ag nanotriangles	210	Not informed	Not informed	Fast coronavirus sensing with simple arrays	Y Yang et al (2022) Ref [48]
Au elliptic nanodisk-rings	440	7 95	Not informed	Enhanced sensing via stacked elliptic-disk–ring design (simulation)	H Bahador et al (2021) Ref [17]
Ag nanorings	524	10	Not informed	Optimized nanoring-coupled design for cancer detection (simulation)	G Abdi et al (2024) Ref [47]
Au nanorings	577	6 1	Not informed	Good sensing by SLR	S Wang et al (2018) Ref [49]
Asymmetric metasurfaces	626 8 502 6	33 5 28 85	Not informed	Enhanced bimodal SLR sensing by complex design	L Li et al (2024) Ref [44]
Au mushroom	1015	80-108	Not informed	Optimized array for achieving FoM near theoretical limit	Y Shen et al (2013) Ref [45]
Au nanoring-on-film	386 615	5 44	Not informed	Sensing via gap and lattice plasmons	Y Liang et al (2018) Ref [46]
Au double-pillar	Not informed	Not informed	17	High-Q sensing via quasi-BICs	Liang et al (2020) Ref [35]

Although our results do not match the peak performance reported in some hybrid or sophisticated metasurface-based sensors, they are comparable with those based on simpler geometries This performance is primarily enabled by the lattice configuration, which supports narrow plasmonic resonances—a clear advantage over isolated nanoparticles While there remains room for further optimization, particularly in terms of nanoparticle geometry, this work demonstrates that significant performance gains are achievable through lattice effects alone, even without intricate nanostructuring or multilayer architectures

4. Conclusions

This study provides a comprehensive analysis of the enhancement of the Q factor and sensitivity in gold nanoparticle arrays, driven by plasmonic surface lattice resonances (SLRs) By employing finite element method (FEM) simulations, we demonstrated that careful control of nanoparticle

Optics EXPRESS

geometry and lattice configuration significantly enhances both the quality factor and optical response, overcoming the limitations of localized surface plasmon resonances (LSPRs) Our theoretical findings reveal that periodic arrays of nanospheres, nanodisks, and nanorods exhibit a substantial improvement in quality factors, exceeding values of 200, due to diffractive coupling effects

Moreover, we performed experiments on different distributions of gold nanodisks to validate such theoretical predictions The experimental results are particularly significant as they demonstrate the direct impact of nanoantenna distribution within the array on their optical response These findings highlight the ability to fine-tune the optical behavior of nanoparticle arrays by altering their distribution and organization In addition, the performed proof-of-concept demonstrated the successful application of these arrays as highly sensitive sensors Specifically, the periodic nanodisk array showcased excellent performance in detecting changes in the surrounding medium These results confirm the viability of the device as a sensor with a sensitivity of 471 nm/RIU, Q factor of 16 6 and a figure of merit of 8 3 RIU ^{1}, values that are in line with state-of-the-art SLR-based systems While some previous studies have reported higher sensitivities using more complex nanoparticle configurations or hybrid nanostructures, our approach demonstrates that a periodic array of simple gold nanodisks can reach a competitive sensitivity This represents a significant enhancement compared to the isolated nanoparticle case and illustrates the powerful role of diffractive coupling in boosting sensor performance The design simplicity and fabrication feasibility of our structure offer practical advantages for scalable biosensing platforms, especially in scenarios where ease of manufacturing and structural reproducibility are essential Overall, this work intentionally focuses on a simple configuration to isolate the effect of periodicity and underlines the potential of SLR-driven gold nanoparticle arrays for use in high-performance (bio) sensing While limited in scope, this case study provides a foundation for future systematic optimization and illustrates the substantial gains enabled by periodic arrangement alone By further optimizing nanoparticle geometries and array configurations, these systems can be tailored to meet the needs of various applications in the biomedical field

Funding. Fundação de Amparo à Pesquisa do Estado de São Paulo (2021/11380–5, 2021/00199–8, 2022/11596-0); Coordenação de Aperfeiçoamento de Pessoal de Nível Superior (PhD student grant); Conselho Nacional de Desenvolvimento Científico e Tecnológico (314539/2023-9); Agencia Estatal de Investigación (10 13039/501100011033); Hezkuntza, Hizkuntza Politika Eta Kultura Saila, Eusko Jaurlaritza; Ministerio de Ciencia, Innovación y Universidades (PID2022-142008NB-I00); Eusko Jaurlaritza (KK-2023/00016); Ministerio de Ciencia, Tecnología e Innovación (112721-461-2023, COD 106532); Universidad Distrital Francisco José de Caldas (CIDC N°01-2023, COD 11-2023); Diputación Foral de Gipuzkoa (QSEIRA project (2024-QUAN-000011-01))

Acknowledgments. A G -E acknowledges IKUR Strategy under the collaboration agreement between Ikerbasque Foundation and DIPC on behalf of the Department of Education of the Basque Government, Programa de Ayuda de Apoyo a los agentes de la Red Vasca de Ciencia, Tecnología e Innovación acreditados en la categoría de Centros de Investigación Básica y de Excelencia (Programa BERC) from the Departamento de Universidades e Investigación del Gobierno Vasco A S acknowledges funding by grant CEX2020-001038-M funded by MICIU/AEI/10 13039/501100011033 M Z -H acknowledges financial support by the Gipuzkoa Quantum program's 2024 call of the Department of Economic Promotion and Strategic Projects of the Provincial Council of Gipuzkoa through the grant awarded to the QSEIRA project (2024-QUAN-000011-01)

Disclosures. The authors declare no conflicts of interest

Data availability. The authors declare that the data are available from the corresponding author on request

Supplemental document. See Supplement 1 for supporting content

References

1 J L Montaño-Priede, M Zapata-Herrera, R Esteban, *et al* , "An overview on plasmon-enhanced photoluminescence via metallic nanoantennas," Nanophotonics **3**(26), 4771–4794 (2024)
2 L Novotny and N van Hulst, "Antennas for light," Nat Photonics **5**(2), 83–90 (2011)
3 J Langer, S M Novikov, and L M Liz-Marzán, "Sensing using plasmonic nanostructures and nanoparticles," Nanotechnology **26**(32), 322001 (2015)

Optics EXPRESS

4 G Baffou and R Quidant, "Nanoplasmonics for chemistry," Chem Soc Rev **43**(11), 3898 (2014)
5 J N Anker, W P Hall, O Lyandres, *et al* , "Biosensing with plasmonic nanosensors," Nat Mater **7**(6), 442–453 (2008)
6 C Clavero, "Plasmon-induced hot-electron generation at nanoparticle/metal-oxide interfaces for photovoltaic and photocatalytic devices," Nat Photonics **8**(2), 95–103 (2014)
7 H Aouani, M Rahmani, M Navarro-Cía, *et al* , "Third-harmonic-upconversion enhancement from a single semiconductor nanoparticle coupled to a plasmonic antenna," Nat Nanotechnol **9**(4), 290–294 (2014)
8 H A Atwater and A Polman, "Plasmonics for improved photovoltaic devices," Nat Mater **9**(3), 205–213 (2010)
9 L Novotny and B Hecht, *Principles of Nano-Optics* (Cambridge University Press, 2012)
10 R M Rowan-Robinson, J Hurst, A Ciuciulkaite, *et al* , "Direction-Sensitive Magnetophotonic Surface Crystals," Adv Photonics Res **2**(10), 2170033 (2021)
11 K Mishra, A Ciuciulkaite, M Zapata-Herrera, *et al* , "Ultrafast demagnetization in a ferrimagnet under electromagnetic field funneling," Nanoscale **3**(46), 19367–19375 (2021)
12 A López-Ortega, M Zapata-Herrera, N Maccaferri, *et al* , "Enhanced magnetic modulation of light polarization exploiting hybridization with multipolar dark plasmons in magnetoplasmonic nanocavities," Light: Sci Appl **9**(1), 49 (2020)
13 C A Herreño-Fierro, E J Patiño, G Armelles, *et al* , "Surface sensitivity of optical and magneto-optical and ellipsometric properties in magnetoplasmonic nanodisks," Appl Phys Lett **08**(2), 021109 (2016)
14 A García-Etxarri, J M Ugalde, J J Sáenz, *et al* , "Field-Mediated Chirality Information Transfer in Molecule–Nanoparticle Hybrids," J Phys Chem C **24**(2), 1560–1565 (2020)
15 F Neubrech, A Pucci, T W Cornelius, *et al* , "Resonant Plasmonic and Vibrational Coupling in a Tailored Nanoantenna for Infrared Detection," Phys Rev Lett **0** (15), 157403 (2008)
16 A García-Etxarri and J A Dionne, "Surface-enhanced circular dichroism spectroscopy mediated by nonchiral nanoantennas," Phys Rev B **87**(23), 235409 (2013)
17 H Bahador and H Heidarzadeh, "A New Proposal for Highly Sensitive Refractive Index Sensor Using Vertically Coupled Plasmonic Elliptic-Disk up Elliptic-Ring Nanoparticles," Plasmonics **6**(4), 1223–1230 (2021)
18 K A Willets, A J Wilson, V Sundaresan, *et al* , "Super-Resolution Imaging and Plasmonics," Chem Rev **7**(11), 7538–7582 (2017)
19 E Ozbay, "Plasmonics: Merging Photonics and Electronics at Nanoscale Dimensions," Science **3** (5758), 189–193 (2006)
20 H C Zhang, L P Zhang, P H He, *et al* , "A plasmonic route for the integrated wireless communication of subdiffraction-limited signals," Light: Sci Appl **9**(1), 113 (2020)
21 A C Atre, A García-Etxarri, H Alaeian, *et al* , "Toward high-efficiency solar upconversion with plasmonic nanostructures," J Opt **4**(2), 024008 (2012)
22 L Mascaretti, Y Chen, O Henrotte, *et al* , "Designing Metasurfaces for Efficient Solar Energy Conversion," ACS Photonics **0**(12), 4079–4103 (2023)
23 Z Zhang, C Zhang, H Zheng, *et al* , "Plasmon-Driven Catalysis on Molecules and Nanomaterials," Acc Chem Res **52**(9), 2506–2515 (2019)
24 A Tittl, H Giessen, and N Liu, "Plasmonic gas and chemical sensing," Nanophotonics **3**(3), 157–180 (2014)
25 J Garciá-Guirado, M Svedendahl, J Puigdollers, *et al* , "Enhanced Chiral Sensing with Dielectric Nanoresonators," Nano Lett **20**(1), 585–591 (2020)
26 Y Y Lee, R M Kim, S W Im, *et al* , "Plasmonic metamaterials for chiral sensing applications," Nanoscale **2**(1), 58–66 (2020)
27 W Ma, L Xu, L Wang, *et al* , "Chirality-Based Biosensors," Adv Funct Mater **29**(1), 1805512 (2018)
28 F Wang and Y R Shen, "General Properties of Local Plasmons in Metal Nanostructures," Phys Rev Lett **97**(20), 206806 (2006)
29 W Rechberger, A Hohenau, A Leitner, *et al* , "Optical properties of two interacting gold nanoparticles," Opt Commun **220**(1-3), 137–141 (2003)
30 N J Halas, S Lal, W-S Chang, *et al* , "Plasmons in Strongly Coupled Metallic Nanostructures," Chem Rev (6), 3913–3961 (2011)
31 E Prodan, C Radloff, N J Halas, *et al* , "A Hybridization Model for the Plasmon Response of Complex Nanostructures," Science **302**(5644), 419–422 (2003)
32 A L Koh, K Bao, I Khan, *et al* , "Electron Energy-Loss Spectroscopy (EELS) of Surface Plasmons in Single Silver Nanoparticles and Dimers: Influence of Beam Damage and Mapping of Dark Modes," ACS Nano **3**(10), 3015–3022 (2009)
33 S R K Rodriguez, A Abass, B Maes, *et al* , "Coupling Bright and Dark Plasmonic Lattice Resonances," Phys Rev X (2), 021019 (2011)
34 V G Kravets, A V Kabashin, W L Barnes, *et al* , "Plasmonic Surface Lattice Resonances: A Review of Properties and Applications," Chem Rev **8**(12), 5912–5951 (2018)
35 Y Liang, K Koshelev, F Zhang, *et al* , "Bound States in the Continuum in Anisotropic Plasmonic Metasurfaces," Nano Lett **20**(9), 6351–6356 (2020)
36 Y Liang, D P Tsai, and Y Kivshar, "From Local to Nonlocal High-Q Plasmonic Metasurfaces," Phys Rev Lett **33**(5), 053801 (2024)

Optics EXPRESS

37 E S A Goerlitzer, R Mohammadi, S Nechayev, *et al* , "Chiral Surface Lattice Resonances," Adv Mater **32**(22), 2001330 (2020)

38 J Černigoj, F Silvestri, L P Stoevelaar, *et al* , "Lattice Resonances and Local Field Enhancement in Array of Dielectric Dimers for Surface Enhanced Raman Spectroscopy," Sci Rep **8**(1), 15706 (2018)

39 M Kataja, T K Hakala, A Julku, *et al* , "Surface lattice resonances and magneto-optical response in magnetic nanoparticle arrays," Nat Commun **6**(1), 7072 (2015)

40 X Yang, G Xiao, Y Lu, *et al* , "Narrow plasmonic surface lattice resonances with preference to asymmetric dielectric environment," Opt Express **27**(18), 25384 (2019)

41 J Lasa-Alonso, D R Abujetas, Á Nodar, *et al* , "Surface-Enhanced Circular Dichroism Spectroscopy on Periodic Dual Nanostructures," ACS Photonics **7**(11), 2978–2986 (2020)

42 S Sarkar and T A F König, "Engineering Plasmonic Hybridization toward Advanced Optical Sensors," Adv Sens Res **3**(1), 2300054 (2024)

43 COMSOL, "COMSOL Multyphisics v 5 2, AB, Stockholm, Sweden http://www comsol com," (n d)

44 L Li and W Wu, "Bimodal surface lattice resonance sensing based on asymmetric metasurfaces," Appl Phys Lett **24**(7), 071701 (2024)

45 Y Shen, J Zhou, T Liu, *et al* , "Plasmonic gold mushroom arrays with refractive index sensing figures of merit approaching the theoretical limit," Nat Commun **4**(1), 2381 (2013)

46 Y Liang, L Li, M Lu, *et al* , "Comparative investigation of sensing behaviors between gap and lattice plasmon modes in a metallic nanoring array," Nanoscale **0**(2), 548–555 (2018)

47 G Abdi and H Bahador, "High sensitivity and optimum design of LSPR-based sensors by coupled nano-rings for cancer detection," Opt Lasers Eng **74**, 107975 (2024)

48 Y Yang, J Murray, J Haverstick, *et al* , "Silver nanotriangle array based LSPR sensor for rapid coronavirus detection," Sens Actuators, B **359**, 131604 (2022)

49 S Wang, X Sun, M Ding, *et al* , "The investigation of an LSPR refractive index sensor based on periodic gold nanorings array," J Phys D: Appl Phys **5** (4), 045101 (2018)

50 K E Chong, H W Orton, I Staude, *et al* , "Refractive index sensing with Fano resonances in silicon oligomers," Phil Trans R Soc A **375**(2090), 20160070 (2017)

51 B Auguié and W L Barnes, "Collective Resonances in Gold Nanoparticle Arrays," Phys Rev Lett **0** (14), 143902 (2008)

52 M W Knight, Y Wu, J B Lassiter, *et al* , "Substrates Matter: Influence of an Adjacent Dielectric on an Individual Plasmonic Nanoparticle," Nano Lett **9**(5), 2188–2192 (2009)

53 M A Mahmoud, M Chamanzar, A Adibi, *et al* , "Effect of the Dielectric Constant of the Surrounding Medium and the Substrate on the Surface Plasmon Resonance Spectrum and Sensitivity Factors of Highly Symmetric Systems: Silver Nanocubes," J Am Chem Soc **34**(14), 6434–6442 (2012)

54 D Sikdar, W Zhu, W Cheng, *et al* , "Substrate-Mediated Broadband Tunability in Plasmonic Resonances of Metal Nanoantennas on Finite High-Permittivity Dielectric Substrate," Plasmonics **0**(6), 1663–1673 (2015)